Evaluation of Bridge Load Carrying Capacity Using
Updated Finite Element Model and Nonlinear Analysis

by

Lina Ding, Hong Hao, Yong Xia and Andrew J. Deeks

Reprinted from

Advances in Structural Engineering

Volume 15 No. 10 2012

MULTI-SCIENCE PUBLISHING CO. LTD.
5 Wates Way, Brentwood, Essex CM15 9TB, United Kingdom

Evaluation of Bridge Load Carrying Capacity Using Updated Finite Element Model and Nonlinear Analysis

Lina Ding[1], Hong Hao[1], Yong Xia[2,*] and Andrew J. Deeks[3]

[1]School of Civil & Resource Engineering, The University of Western Australia, Crawley, WA 6009, Australia
[2]Department of Civil & Structural Engineering, The Hong Kong Polytechnic University, Hong Kong, China
[3]School of Engineering and Computing Sciences, Durham University, Durham, UK

(Received: 8 January 2010; Received revised form: 6 February 2012; Accepted: 14 February 2012)

Abstract: The integrity of ageing bridges is in doubt because of increasing traffic loads, deterioration of materials, possible damage during service, and revised code requirements. Traditional methods in prediction of load varying capacity of bridges are usually based on the design blueprints and may not reflect the bridge condition as is. In this paper, the nonlinear finite element analysis, incorporating the model updating technique, is used to predict the behaviour of a 30-year-old slab-girder bridge. The original finite element model based on the design drawings is updated by modifying the stiffness parameters of the girders, slab, shear connectors and bearings so that the vibration properties of the model match the field vibration measurement data. The updated model represents the present condition of the bridge better than the original model that is based on the design blueprints. The load carrying capacity of the bridge is then calculated using the original and updated finite element models, respectively, with consideration of nonlinear material properties. The comparison shows that the bridge load carrying capacity under the present condition is lower than that under the design condition, whereas is still above the design requirement. The influence of the shear connectors on the load carrying capacity is specially investigated.

Key words: slab-girder bridges, load carrying capacity, nonlinear finite element analysis, model updating, shear connector.

1. INTRODUCTION

The load carrying capacity of bridges affects the serviceability, traffic safety, and transportation costs directly. It tends to decrease over years of service, due to physical damage caused by factors such as over loading, accidental impact, or material deterioration. On the other hand, increasing vehicle loading requires a higher load carrying capacity. To deal with this dilemma and to avoid the huge cost of repairing, upgrading or replacing existing bridges, accurate assessment of the load carrying capacity of bridges is becoming more and more important.

In many countries, including Australia, standard methods are provided for rating existing bridges. These methods are only an extension of design rules, and usually lead to conservative results. Much research has been carried out to improve the accuracy of load carrying capacity prediction. Stallings and Yoo (1993) refined the load rating procedure by predicting the wheel-load distribution factor from the stationary truck test and the impact factor from the moving truck test. Cai and Shahawy (2003) and Chowdhury and Ray (2003) developed methods to estimate the load distribution factors based on field test data. Azizinamini *et al*. (1994) used yield line analysis with material properties obtained from laboratory tests to estimate the bridge load carrying capacity. Barker (1995) employed the shakedown limit rating method, which included a more realistic load distribution, and considered both the inelastic system limit state and the bridge system

*Corresponding author. Email address: ceyxia@polyu.edu.hk; Fax: 852-2334-6389; Tel: 852-2766-6066.
Associate Editor: S.S. Law.

redistribution of forces in the longitudinal and transverse directions. Ghosn *et al*. (1986) used diagnostic results at controlled loads much below the service loads to extrapolate the performance of a bridge at design loadings. They verified the new bridge testing methods in Switzerland, and extended these methods to the strength evaluation. The method is a compromise between a diagnostic performance test and a proof loading check on capacity. Nowak and Tharmabala (1998) used test data to improve the accuracy of load and resistance models. Studies on bridge evaluation with non-destructive field test methods were carried out by Chajes *et al*. (1997), Scott *et al*. (2003), and Rens *et al*. (2005).

With the rapid development of computer capability and finite element methodology, research that combine field tests and finite element analysis for bridge load carrying capacity prediction has become popular during the last two decades. Law *et al*. (1995) derived the best estimation of the moment of inertia of a girder by fitting the first frequency of the finite element model and the test results. Chajes *et al*. (1997) used diagnostic testing results to determine the composite section properties of the girders and support restraints, and then to develop a numerical model of the bridge to estimate the maximum allowable load. Jauregui and Barr (2004) developed an equivalent frame model to calculate the load distribution factor for bridge load rating by comparing the moment distribution in the longitudinal direction obtained from different finite element models with the field test data. Brownjohn and Xia (2000) introduced the sensitivity-based model updating method into the structural condition assessment procedure. This method was later applied to real bridges to update the bridge models for condition assessment (Brownjohn *et al*. 2001).

However, most of the research on load carrying capacity is limited to linear analysis of bridges or nonlinear analysis of bridge components. Nonlinear finite element analysis for load carrying capacity of real bridges is still rare because of heavy computational load. In addition, ageing bridges may be deteriorated after many years service. Their capacity may not suffice the new traffic condition. In this paper, the nonlinear finite element analysis and the model updating technique are combined to assess the behaviour of an existing slab-girder bridge in Western Australia. The field vibration testing data are used to update the finite element model. The updated model is then used to perform nonlinear analysis and predict the bridge load carrying capacity under the present condition. The effectiveness of the nonlinear finite element analysis is verified through the comparison with a benchmark example by Rabczuk and Eibl (2004). The load carrying capacity of the bridge using the original and updated models is predicted respectively and compared. The effect of shear connectors condition on the load carrying capacity is investigated.

2. THE BRIDGE CONSIDERED IN THIS STUDY

In Western Australia, about 50 bridges were built in the mid 1970's in the Pilbara region, each based on the same design blueprints. After more than 30 years of service, especially after experiencing several floods, the bridge authority is keen to know the current condition and the load carrying capacity of the bridges.

The bridge under study, Bridge No. 852 as shown in Figure 1, is located North West Coastal Highway over the Balla Balla River in the Shire of Roebourne, Western Australia. This 30+ year old slab-girder bridge comprises three spans with seven precast prestressed concrete girders and a cast-in-situ slab. The side spans are 17.84 m long and the central span is 18.29 m. Figure 2 shows the dimensions of the bridge deck. The slab is 9.14 m wide accommodating two traffic lanes and 140 mm thick on average. Details A and B respectively show the reinforcement of the slab and the girder in the middle of the span. The slab and girders are integrated by shear connectors in the span and diaphragms on the supports.

The visual inspection in August 2004 indicated that the entire structure was still in good condition, although significant transverse cracks were found throughout the kerbs on both sides of the bridge and some longitudinal cracks on girders of one side span. However, the condition of the shear connectors and the actual load carrying capacity of the bridge under the present condition, which are difficult to measure with visual inspection and the rating method in design codes, are not known. Because of the increasing traffic loads, the revised code requirements, and possible damage caused by floods, it is important to evaluate the bridge

Figure 1. General view of bridge No. 852

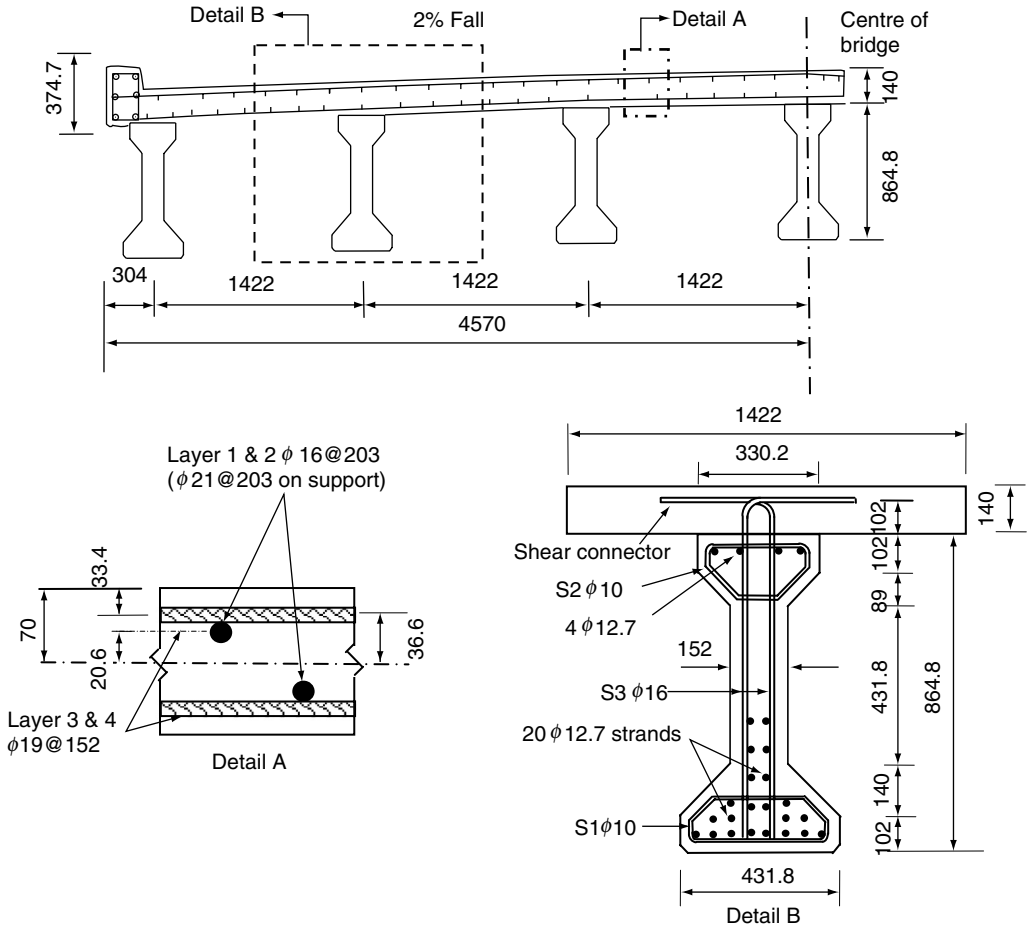

Figure 2. Dimension of the bridge deck and the reinforcement in the middle span (unit: mm)

conditions and its current load carrying capacity accurately. For these purposes, field vibration tests were carried out in late September 2004 and again in early October 2005 (Xia *et al*. 2007, 2008). The field test data will be used in this study to update the finite element model and assess the performance of the bridge.

3. MATERIAL MODELS AND VERIFICATION

Nonlinear behaviour of steel and concrete are important properties in the analysis of structural performance, especially in predicting a structure's ultimate load carrying capacity. However, even now, nonlinear finite element analysis is still usually limited to structural members. The elastic assumption is normally assumed in the finite element analysis of large-scale structures. This is because nonlinear finite element analysis not only substantially increases computational effort, but also requires advanced material models that can simulate the complicated concrete behaviour and the interaction between concrete and reinforcement. In recent years, with the development of computer capability, nonlinear finite element analysis has been applied to large-scale complicated structures. With proper concrete constitutive models, a number of studies have demonstrated the potential and reliability of the nonlinear finite element method for analysis of concrete structures (Balakrishnan and Murray 1988; Lee and Fenves 1998; Wang and Hsu 2001; Rabczuk and Eibl 2004).

The reliability of the finite element model analysis relies on the accuracy of the material models. In this study, the plasticity model is used for reinforcement and the damage plasticity model for concrete. The validity of these models for predicting the performance of a prestressed concrete structure at its ultimate condition is verified by application to a benchmark laboratory test by Rabczuk and Eibl (2004).

3.1. Material Models

A plasticity model with strain hardening in both tension and compression is used to model the reinforcement. The bond between the concrete and reinforcement is assumed to be perfect. A concrete damage plasticity model is used to model the behaviour of concrete. It uses isotropic damage elasticity in combination with isotropic tensile and compressive plasticity to represent the inelastic behaviour of concrete.

3.1.1. Concrete in compression

The relationship for compression branch (Figure 3) is determined from Eqns 1 and 2 (Krauthammar and Hall 1982; Balakrishnan and Murray 1988). In this model, the stress-strain relationship is linear until the initial yield value of 0.9 times the compressive strength, f_{cm}. It then exhibits strain hardening, and followed by softening after the peak value f_{cm}.

$$E_1 = 0.05E_0 \tag{1}$$

$$E_2 = -0.018E_0 \tag{2}$$

where E_0 is the Young's modulus of the concrete.

3.1.2. Concrete in tension

Under the uni-axial tension, the stress-strain response follows a linear elastic relationship until the value of the failure stress, f_{cr}, is reached, which is expressed as Eqn 3:

$$\sigma_1 = E_0\varepsilon_1, \varepsilon_1 \le \varepsilon_{cr} \tag{3}$$

The failure stress corresponds to the onset of micro-cracking in the concrete material. After cracking, concrete is still capable of resisting tensile forces partially due to the bond slip and dowel action between the concrete and reinforcement. This phenomenon, resulting from crack formation and the bond between steel and its surrounding concrete, is defined as the tension stiffening effect (Kwak and Kim 2001). In this study, a constitutive model that combines the model proposed by Wang and Hsu (2001) and the model in ABAQUS (2003) is used. The descending branch consists of two parts (Figure 3). The curve from A to B is described by Eqn 4, and the stress-strain relationship from B to C is linear. The position of point C is determined by Eqn 5 (ABAQUS, 2003).

$$\sigma_1 = f_{cr}\left(\frac{\varepsilon_{cr}}{\varepsilon_1}\right)^{0.4} \quad \varepsilon_1 > \varepsilon_{cr},\ \sigma_1 \ge 0.5f_{cr} \tag{4}$$

$$\sigma_1 = 0, \varepsilon_1 = 50\varepsilon_{cr} \tag{5}$$

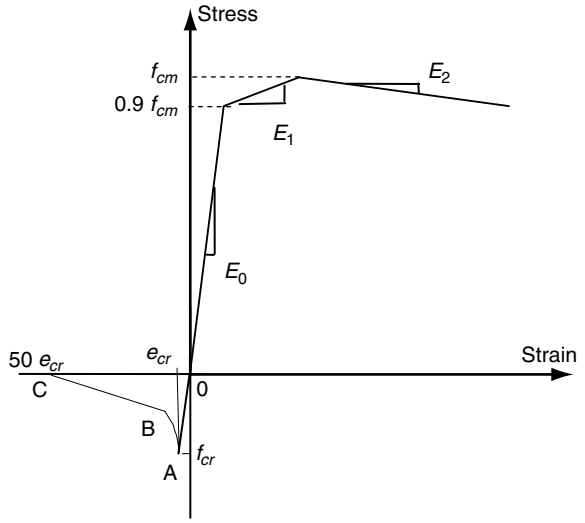

Figure 3. Uni-axial compression and tension stress-strain relationship for concrete

3.2. Model Verification

3.2.1. Example beam

To verify the accuracy of the material model described above, the nonlinear finite element analysis is used to predict a laboratory test reported in the literature (Rabczuk and Eibl 2004). The experimental model is a simply supported rectangular beam, as shown in Figure 4. The beam was prestressed with two tension wires of 7 mm diameter: the lower one was prestressed with a force of 26.25 kN, and the upper one with a force of 11.25 kN.

For the concrete, the elastic modulus is 29 GPa, the compression strength is 44.5 MPa, the tensile strength is 2.83 MPa, the Poisson's ratio is 0.22, and the density is 2400 kg/m^3. For the reinforcement, the yield point of the tension wires is 1470 MPa, the tensile strength is 1670 MPa, the Young's modulus is 200 GPa, and the density is 7800 kg/m^3.

3.2.2. Results and comparison

C3D8R eight-node linear solid elements in ABAQUS are used to discretise the beam. SFM3D4R four-node quadrilateral elements are used to model the rebar layer, which is embedded in the solid elements. No slip between the concrete and the rebar layers is assumed. Four different mesh schemes, as shown in Figure 5, are used to investigate the sensitivity of the finite element

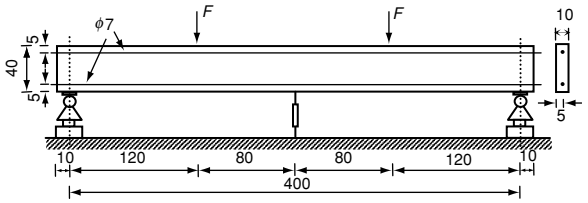

Figure 4. Tested prestressed beam (unit: mm)

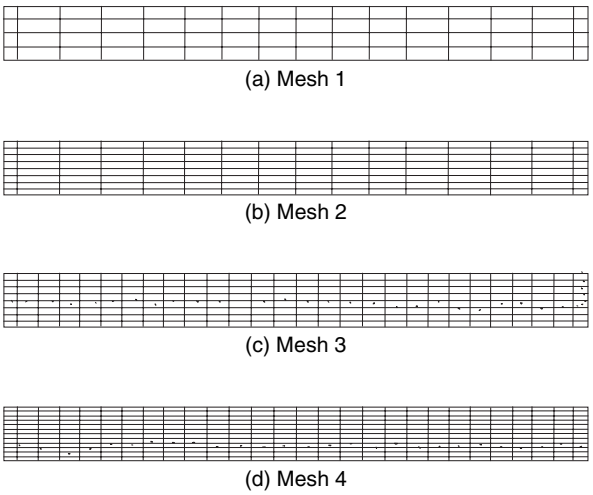

Figure 5. Finite element model of the benchmark beam with different mesh schemes

analysis to the mesh size in longitudinal and vertical directions. Table 1 summarises the number of elements for each mesh scheme. The load-deflection curves are calculated from the nonlinear finite element analysis and compared with the laboratory test results, as shown in Figure 6.

Table 1. Summary on meshes of the benchmark beam

Element number	Vertical	Longitudinal	Total
Mesh 1	4	16	64
Mesh 2	8	16	128
Mesh 3	8	28	224
Mesh 4	12	28	336

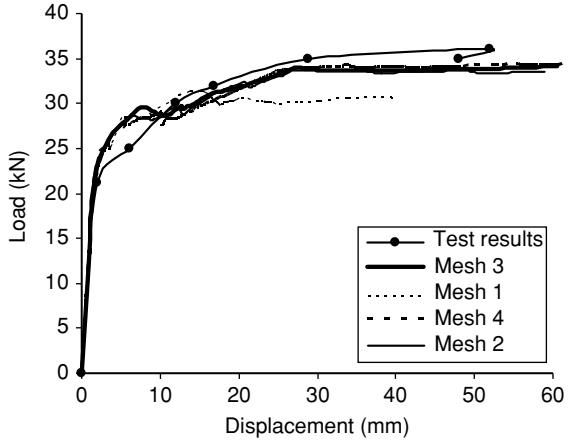

Figure 6. Load-displacement relationship

It can be seen that the results calculated from the coarse mesh, Mesh 1, predict the initial response of the beam accurately, whereas deviate from the test results with the growth of cracks in concrete and yielding in strands. This results in an underestimation of the load carrying capacity. Mesh 2 uses twice elements in the vertical direction and same number of elements in the longitudinal direction as Mesh 1. As shown, the results from Mesh 2 match the test results better. Further, Mesh 3 increases the element number in the longitudinal direction and Mesh 4 increases the mesh density in the vertical direction. Their load-displacement curves are close to that of Mesh 2. Therefore, Mesh 2 is sufficient to model the beam. It is also found that the analysis results are more sensitive to the mesh density in vertical direction than in the longitudinal direction, which indicates that it is reasonable to use a coarse mesh in the longitudinal direction to reduce the computation cost.

The above results demonstrate that the nonlinear finite element analysis and the associated material constitutive models can provide an accurate estimation of the load carrying capacity of the prestressed concrete beam. The material models will be used to analyse the bridge under consideration.

4. FINITE ELEMENT MODEL OF THE BRIDGE BASED ON DESIGN DRAWINGS

A three-dimensional finite element model is built according to the design drawings, as shown in Figure 7. Alphabets A to G indicate the transverse position of the girders and the bearings.

4.1. Material Parameters

The 7-wire steel strand used in the concrete girders is assumed to be an elastic-plastic material, with a bilinear stress-strain relationship. Its initial Young's modulus is 195 GPa, tensile strength f_p is 1750 MPa (AS1311 1987),

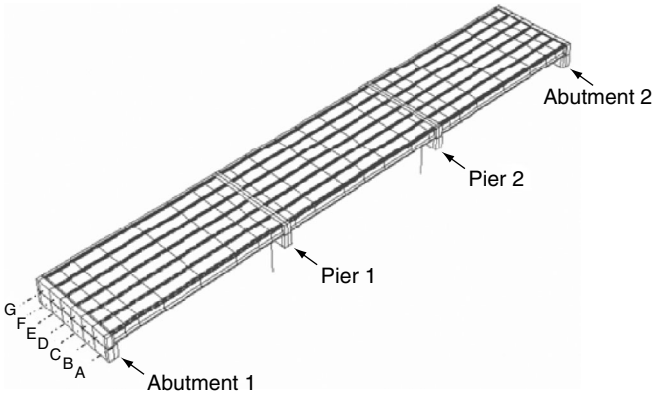

Figure 7. Finite element model of the bridge

yield strength is taken as $0.85f_p$, 1487.5 MPa, ultimate strain is taken as 3.5 percent, and density is 7900 kg/m^3. The design prestressing force is 84.78 kN per strand. The reinforcements in the slab and top of the girders are cold-formed bars. According to AS 1302, the yield strength, f_{sy}, is taken as 500 MPa and the modulus of elasticity is taken as 200 GPa.

Concrete density is 2500 kg/m^3. Its compression strength is 31.0 MPa for the slab and 48.3 MPa for the girders. The Young's modulus of concrete is calculated from Eqn 6, which is 29.4 GPa for the slab and 37.4 GPa for the girders. Poisson's ratio is 0.20. The tensile strength, f_{cr}, is calculated from Eqn 7 (AS5100 2004), which is 2.17 MPa for the slab and 2.44 MPa for the girders. The columns, diaphragms, and slab use the same concrete parameters.

$$E_0 = \rho^{1.5} \times 0.043 \times \sqrt{f_{cm}} \tag{6}$$

$$f_{cr} = 0.4 \times \sqrt{f_{cm}} \tag{7}$$

4.2. Modelling of the Superstructure

The concrete slab is modelled by three dimensional four-node shell elements with four rebar layers. The parameters defining the rebar layers of the slab in the mid span are listed in Table 2. Additional reinforcement is placed over the support to resist the negative moment. The prestressed I-section girders are discretised by eight-node solid elements with embedded rebar layers. Each girder has 22 strands and four reinforcements, which are simulated by four rebar layers, as shown in Figure 8 and listed in Table 3. Figure 9 illustrates the elevation of the rebar layers in a typical girder. All the rebar layers are modelled with surface (quadrilateral) elements. There are 81 shear connectors for each girder over each span, and 1701 in total for the bridge. To reduce the finite element model size, a cluster of shear connectors are lumped together based on the area equivalent, which results in seven equivalent stirrups on each girder over each span. Each equivalent shear connector is modelled by a CARTESIAN connector element, providing a connection between two nodes at

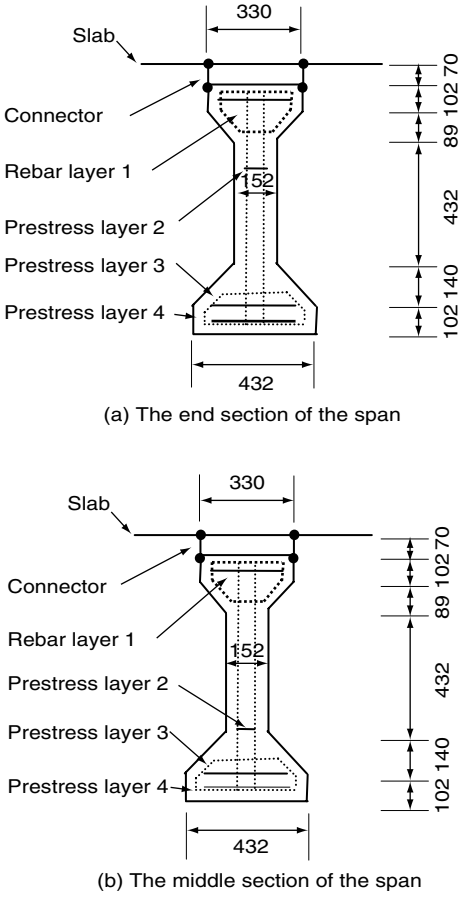

Figure 8. Rebar layers in girder section (mm)

Table 3. Rebar layers in the girders of the bridge

Layer	Number	Diameter	Area per bar
1	4	12	201
2	8	12.7	94*
3	8	12.7	94
4	6	12.7	94

Note: * According to the Australian Standard AS1311-1987, the nominal area of the 12.7 mm diameter strand used in girders is 94 mm^2.

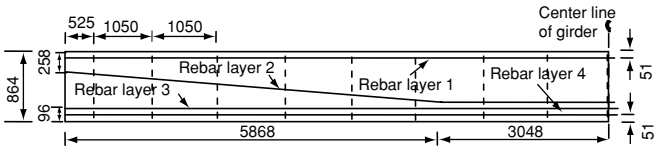

Figure 9. Elevation view of a girder (mm)

Table 2. Rebar layers in the slab of the bridge

Layer	Orientation	Number	Area per bar (mm^2)	Spacing (mm)
1	Longitudinal	41	201	203.2
2	Longitudinal	41	201	203.2
3	Transverse	360	285	152.4
4	Transverse	360	285	152.4

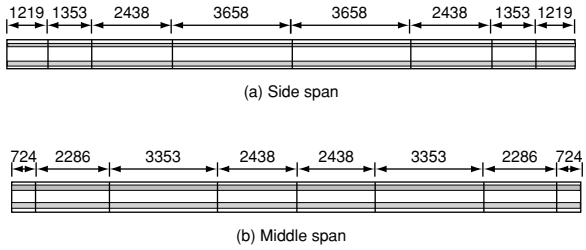

Figure 10. Location of shear connectors

the slab and girders. The locations of the lumped shear connectors are shown in Figure 10. The accuracy and efficiency of this simplification was verified by Xia *et al*. (2008). The three dimensional two-node truss elements, T3D2, are used to model stirrups. The dashed lines in Figure 9 denote the location of the simulated stirrups in the girder. The stirrups in every 1.05 m are lumped together to form an equivalent stirrup, which results in 17 stirrups in each girder over each span.

4.3. Boundary Conditions

The field observations indicated that the columns of the abutments are buried and unlikely to move due to the resistance of the soil and rocks around the abutment. Consequently the columns of the abutments are not included in the finite element model. The cap beams over the abutments are restrained directly as simply supported in the model. The cap beams over the piers are supported by two 3.81 m long RC columns of 0.6 m diameter. Each column in the piers is supported by a square pad footing, which provides enormous resistance to the column. Consequently, the columns are assumed to be restrained at the ground level and are modelled by beam elements, B31.

The superstructure is supported by rubber bearings at the piers and the abutments. The bearings are assumed to behave elastically and modelled by CARTESIAN connector elements. The Young's modulus of the bearings is 0.2 GPa according to the design datasheet.

4.4. Convergence Study

A convergence study is carried out to find a proper mesh and achieve the balance between the accuracy and the computational time. For efficiency, a representative girder is selected for the mesh convergence study. The girder is simply supported and subjected to a concentrated load at the middle. As discussed before, the mesh size in the vertical direction can be much smaller than that in the longitudinal direction. Five different mesh schemes are tested. The element numbers are 4, 8, and 14 in the vertical direction and 8, 14, 28, and 52 in the longitudinal direction. Displacement at the mid-span

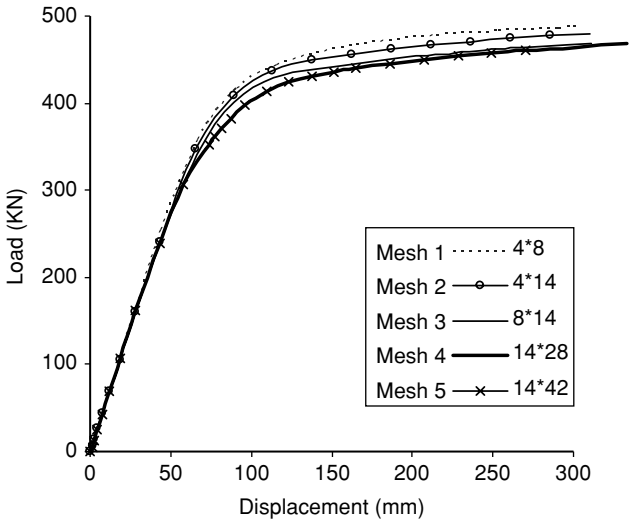

Figure 11. Load-displacement curves for different meshes

is calculated for each scheme and shown in Figure 11. It can be found that the analysis converges in the cases of Nos. 4 and 5, and the difference between No. 3 and No. 4 is very slight. Therefore, the mesh density of No. 3 is regarded sufficient for analysis of this girder and will be adopted in the following numerical analysis.

4.5. Traffic Load Model

The bridge was designed according to the old Australian standard nearly 30 years ago. In order to evaluate the capacity of the bridge under the current traffic condition, the new traffic load standard, AS5100 (2004), is adopted. The M1600 vehicle load in AS5100, shown in Figure 12, is selected as the critical load model. It consists of a uniformly distributed load together with truck wheel loads. The former is uniformly distributed over a width of 3.2 m standard design lane. The latter is treated as

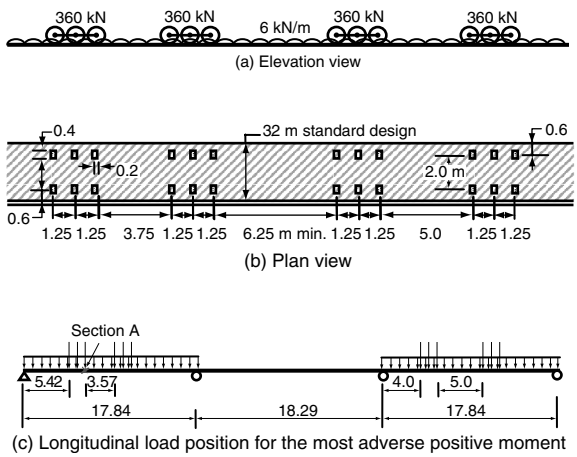

Figure 12. M1600 moving traffic load

Table 4. Live load effects of the nominal traffic loads

	Wheel load	Distributed component
First	140.4 KN	4.39 KN/m^2
Second	112.3 KN	3.51 KN/m^2

concentrated loads. The deck between the kerbs is 8.5 m wide and accommodates two traffic lanes. The wheel loads for the first lane are located on the second girder to produce the maximum response in this girder. The second traffic lane is positioned 1.2 m away from the first one.

The live load effects of the nominal vehicle for load rating, L_{RV}, is

$$L_{RV} = \gamma_L (1+\alpha) \sum_{i=1}^{n} W_i S_i^L \tag{8}$$

where n is the number of the design lanes; live load factor γ_L is selected as 1.8; W_i is the accompanying lane factor, which is 1.0 for the first lane and 0.8 for the second; the dynamic allowance, α, is 0.3; and S_i^L is vehicle load. The magnitudes of the traffic loads used for the load carrying capacity analysis are listed in Table 4.

The traffic loads are placed at different positions to obtain the most adverse positive and negative moments. The maximum positive moment is calculated as 7568 kN·m when the first and third spans are loaded, and the minimum negative moment is –8625 kN·m when the first and second spans are loaded. The position of the adverse load is illustrated in Figure 12(c).

5. ULTIMATE LOAD CARRYING CAPACITY EVALUATION

5.1. Load Carrying Capacity Calculated from Empirical Formulae

The moment capacity of the bridge is firstly estimated using empirical formulae (Warner 1998) which are widely adopted in practice. The empirical formulae assume that the plane sections remain plane and the concrete carries no tensile stress. The moment capacity for the composite section is calculated as 2573.8 kN·m in the middle of the span and –3734.4 kN·m on the interior supports. The load distribution factor for the moment is calculated as 0.25, according to the formula suggested by AASHTO (1994). Consequently, the ultimate positive moment capacity of the whole bridge is 10295 kN·m, and the ultimate negative moment capacity is –14937 kN·m on the interior supports. As compared with the load action described in Section 4.5, the bridge capacity is governed by the positive moment capacity and it can carry 1.36 times of the nominal traffic load. The load condition to produce the most adverse positive moment will also be applied to the following nonlinear finite element analysis.

5.2. Finite Element Analysis Using the Original Model

The finite element analysis is carried out in ABAQUS to predict the load-displacement curve of the bridge by increasing the load proportionally. The loading sequence is divided into three stages: prestressing, dead load, and static traffic loads. Newton iteration method is used in the first and second stages, whereas Riks method (Crisfield 1981) is employed in the third stage to avoid computational instability. The load increment is automatically selected by the program. According to AS5100 (2004), the live load factor is 1.8 for the ultimate limit state and 1.0 for the serviceability limit state.

To investigate the effect of shear connectors on the bridge load-carrying capacity, the shear connectors are modelled with three different conditions. The first one assumes that the connection between the slab and the girder is rigid, which corresponds to the assumption of the empirical formula. The second scenario uses the design parameters to model the shear connectors. The shear connectors are damaged completely in the third scenario. The load-displacement curves under the traffic loads for three scenarios are calculated and compared in Figure 13, in which the vertical axis represents the ratio of the applied traffic load to the nominal load and the horizontal axis is the maximum displacement in the girders.

In the first case of rigid connection, the nodes on the slab are tied to the corresponding nodes on the girders, indicating no relative displacement between the slab

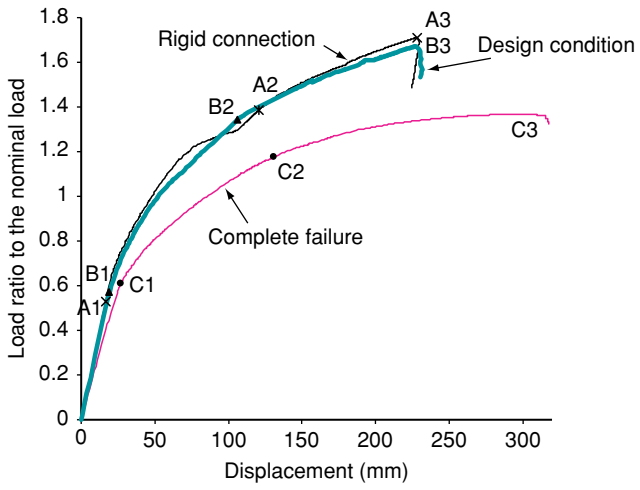

Figure 13. Load-displacement curves for different conditions of shear connectors

and the girders. The maximum stress occurs in the first span of Girder B, as expected from the influence line analyses. The first crack occurs in the middle of Girder B at 0.53 times the nominal load, denoted as A1 in Figure 13. The reinforcement reaches the yielding stress at 1.38 times the nominal load, which is denoted as A2. The maximum vertical displacement of the bridge corresponding to this stage is 120.82 mm. Following further increase of the load, the concrete in the slab crushes at 1.71 times the nominal load (A3). The calculation becomes unstable at this point and the load starts to decrease. These observations indicate that the response is consistent with the assumption in empirical formula that the strands yield before the ultimate load is reached. The load carrying capacity from the finite element analysis is 26% larger than the empirical formula results. There are two main reasons for this:

(1) The load redistribution among the girders is ignored in the empirical formula calculation;
(2) The post yielding stress of the strand is neglected in the empirical formula, whereas strain hardening is considered in the present finite element analysis.

The bold curve in Figure 13 is the load-displacement curve in which the shear connectors in the design condition are modelled. As compared with the rigid connection case, the initial stiffness of the structure decreases by 4.9%. The flexure cracks first occur at 0.57 times the nominal load (point B1). At this time, the stress of the bottom layer strands is 1042 MPa in the cracking section. Then the stress of the strands increases to 1487.5 MPa at 1.34 times the nominal load with 110 mm displacement (point B2). The maximum load that the structure can carry before softening is 1.67 times the nominal load (B3), which is only 2.4% smaller than the rigid connection condition, indicating that the designed shear connectors provide the sufficient connection between the slab and the girders. The load carrying capacity in the design condition is 23% larger than the empirical formula result.

In the third case, all shear connectors are damaged completely. The girders and the slab are connected together by the diaphragms only. There is little shear transfer between the slab and girders, and composite action of the slab and girders no longer exists. Consequently the stiffness of the bridge and load carrying capacity reduces. Figure 13 shows that the initial stiffness of the bridge decreased by 25.3%. The strands start to yield at 1.17 times of the nominal load (C2). The load carrying capacity is 1.36 times the nominal load (C3), approximately 20% lower than that in the second case. This implies that the load carrying capacity of the bridge will decrease by 20% if all shear connectors fail completely.

In all of these scenarios, the changing shear connector properties do not affect the failure pattern. The cracks always occur in the middle of the first span and in the web near the support. With the increase of the loads, the cracks develop and the strands in the cracked section yield first. The failure finally occurs because of crushing in the slab concrete.

5.3. Finite Element Analysis Using the Updated Model

As the actual condition of the bridge may differ from the designed one, using the design blueprints cannot predict the realistic load carrying capacity of the bridge. With the model updating technique, the original model based on the design blueprints can be improved to match the field measurement data. The updated model represents the present condition of the bridge better and consequently gives more accurate estimation of the load carrying capacity.

5.3.1. Model updating

The field tests were carried out in 2004 and 2005 (Xia *et al*. 2008). Hammer impact was used as the excitation source. Accelerometers were employed to measure the dynamic responses at 133 points, from which 11 frequencies and mode shapes were obtained for updating the original model.

The objective function is the combined error of frequencies and mode shapes between analysis (denoted as "*A*") and experiments (denoted as "*E*") (Hao and Xia 2002), expressed as follows:

$$J(p) = \sum_{i=1}^{nm} C_{\lambda i}^2 \left[\lambda_i(\{p\})^A - \lambda_i{}^E \right]^2 + \sum_{i=1}^{nm} C_{\phi i}^2 \sum_{j=1}^{np} \left[\phi_{ji}(\{p\})^A - \phi_{ji}{}^E \right]^2 \quad (9)$$

where λ_i is the i^{th} eigenvalue; $\{\phi_{ji}\}$ are the j^{th} component of the i^{th} mode shape; C is the weight coefficient representing the contribution of each item; and p is a vector of the structural parameters to be updated, here are stiffness parameters of the girders, slab, bearings, and the shear connectors, 857 in quantity. During the model updating, only the measured np points (np = 133 here) and nm modes (nm = 11) are chosen out of the full set of numerical mode shapes for comparison. The weight coefficient is set to 0.1 for mode shapes and 1.0 for frequencies as the measured mode shapes are usually less accurate than the frequencies by one order (Hao and Xia 2002).

The updating process is to minimise the objective function. It converges with 155 iterations using the MATLAB optimisation toolbox (MATLAB 2005). It should be noted that updating a large number of parameters independently may lead to an ill-conditioned inverse problem and often converges to a local minima in the objective function. Local search methods cannot guarantee the converged results are globally optimised solution, whereas global search methods like genetic algorithms are usually very time consuming. The trust-region method, a local optimisation algorithm which is very efficient for large-scale optimisation problems, is employed here. The model updating results, defined as parameter change proportion after and before updating, are plotted in Figure 14. The white bars denote positive values and the black bars denote negative values.

Figure 14(a) shows the stiffness change ratio in each super element of the girders. The change ratio is evenly distributed in the mid span and part of the side spans at around 40%, implying that the stiffness of girders is underestimated in the original finite element model. As the geometric dimension of the elements is regarded as accurate, stiffness change is equivalent to change in Young's modulus of these elements in the updated model. The compressive and tensile strengths are then calculated according to Eqns 6 and 7, given the Young's modulus.

The change of the deck stiffness is illustrated in Figure 14(b). The stiffness of the kerbs increases in the updated model, indicating that the kerb stiffness in the original model is underestimated. The extra stiffness may come from the guardrail, which is not taken into account in the original model. The decrease of stiffness in most parts of the slab shows that the deck deteriorated after 30 years of service. The field inspection shows some cracks in the deck, possibly due to over loading or temperature effects. In the updated model, the weakened slab elements are equivalent to decrease of Young's modulus. Consequently the concrete strengths are calculated according to Eqns 6 and 7.

Figure 14(c) shows the change of the bearing stiffness. The modulus in the original model is determined according to the datasheet in design drawings. After model updating, the stiffness of most bearings on the piers decreases by between 40% and 60%. The stiffness of the bearings on the abutments changes around –20% and 20%, respectively. In Figure 14(d), the change ratio of the stiffness of the shear connectors is quite variable. Significant damage in some shear connectors is observed.

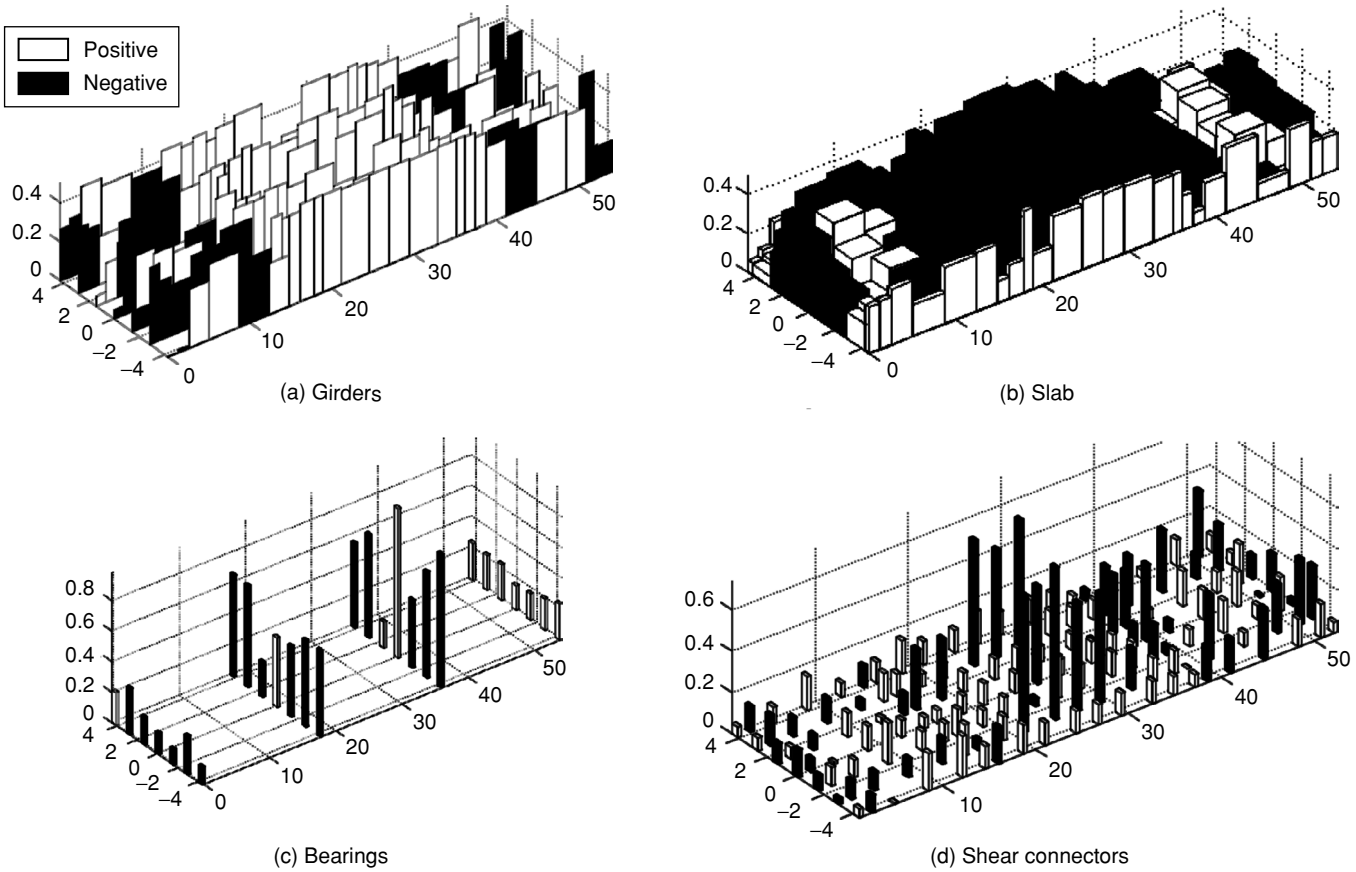

Figure 14. Stiffness change ratio in the updated model

5.3.2. Finite element analysis using the updated model

The updated stiffness parameters are employed in the updated model, and the load-displacement of the updated model is similarly calculated and compared with the results of the original model, as shown in Figure 15.

The figure shows that the initial stiffness of the structure increases by 12%. The decrease of stiffness in the slab elements is counteracted by increase of the stiffness in most parts of the girders. As compared with the cracking mechanism in the original model, shear cracks instead of flexure cracks first appear near the interior support at 0.62 times the nominal load (point D1). Subsequently the flexure cracks appear in the middle of the first girder over the first span at 0.80 times the nominal load (point D2). At this time the displacement is 20.87 mm and the stress of the bottom strands in this section is 998 MPa. The strands start to yield at 1.39 times the nominal load in middle of the first span with 159 mm deflection (point D3). As compared with the original model, more shear cracks develop in the updated model. The stress of the inclined steel strands near the support is 1420 MPa at 1.39 times of the nominal load. Crushing of the concrete in the girders and slab finally causes computational instability. The calculation stops at 1.49 times of the nominal load as the flexure failure happens. The load carrying capacity in the present condition is 12% smaller than the result using the original finite element model. Nevertheless, it is still higher than that from the empirical formula by 10% and can suffice the design requirement of resisting the current traffic load.

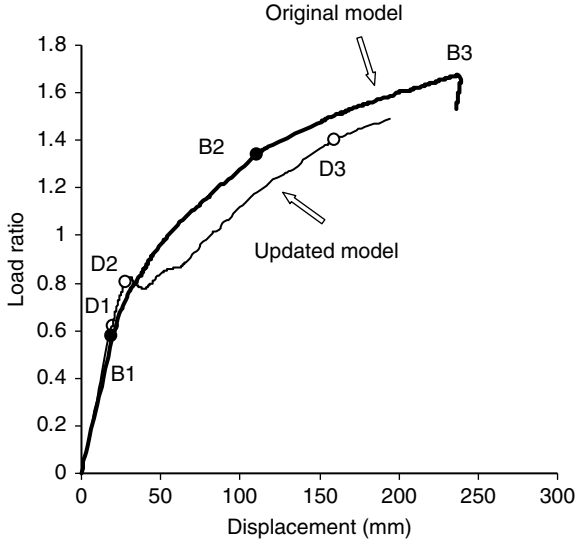

Figure 15. Load-displacement curves of the original and updated models

6. CONCLUSIONS

The nonlinear finite element analysis and model updating method are combined to calculate the load carrying capacity of a slab-girder bridge in this paper.

In the nonlinear analysis, a bilinear elastic-plastic model is used to model the reinforcement, and a damage plasticity model is used for the concrete. The material models are verified with application to a benchmark example. The load-displacement curve shows that the nonlinear finite element analysis can capture the main characteristics of a reinforced concrete member at the ultimate load condition.

The nonlinear finite element analysis is then applied to evaluate a real global bridge. The analysis carried out on the original model shows that the load carrying capacity of the bridge is 1.67 times the ultimate load specified in the design code and 20% higher than the capacity calculated according to the empirical formula. This indicates that the empirical formula underestimates the load carrying capacity of bridges. The finite element model is then updated based on the field vibration tests. The nonlinear analysis on the updated model indicates that the bridge ultimate load carrying capacity is about 1.49 times the nominal load, implying the bridge is still safe under the present traffic condition, whereas 12% less than that estimated from the design model. This exercise demonstrates that the updated model can represent the actual condition of the bridge better and the load carrying capacity based on the updated model can provide a more realistic condition of the bridge.

ACKNOWLEDGEMENT

The first author would like to thank the University of Western Australia (UWA) for the IPRS, UPA, and APA scholarships to pursue a PhD study in UWA.

REFERENCES

AASHTO (1994). *LRFD Bridge Design Specifications*, 1st Edition, American Association of State Highway and Transportation Officials, Washington, D.C., USA.

ABAQUS (2003). *ABAQUS Theory Manual*, Version 6.4, Hibbit, Karlsson and Sorensen, Inc., USA.

AS5100 (2004). *The Australian Standard for Bridge Design*, Standards Australia, Sydney, Australia.

AS1302 (1991). *The Australian Standard for Steel Reinforcing Bars for Concrete*, Standards Australia, Sydney, Australia.

AS1311 (1987). *The Australian Standard for Steel Tendons for Prestressed Concrete –7-Wire Stress-Relieved Steel Strand for Tendons in Prestressed Concrete*, Standards Australia, Sydney, Australia.

Azizinamini, A., Shekar, Y., Barnhill, G. and Boothby, T.E. (1994). "Old concrete slab bridges: Can they carry modern traffic loads?", *International Concrete*, Vol. 16, No. 2, pp. 64–69.

Balakrishnan, S. and Murray, D.W. (1988). "Concrete constitutive model for NLFE analysis of structures", *Journal of Structural Engineering*, ASCE, Vol. 114, No. 7, pp. 1449–1466.

Barker, M.G. (1995). "Load rating and ultimate capacity evaluation of compact steel girder bridges", *Transportation Research Record*, No. 1476, pp. 1–7.

Brownjohn, J.M.W. and Xia, P.Q. (2000). "Dynamic assessment of a curved cable-stayed bridge by model updating", *Journal of Structural Engineering*, ASCE, Vol. 126, No. 2, pp. 252–260.

Brownjohn, J.M.W., Xia, P.Q., Hao, H. and Xia, Y. (2001). "Civil structure condition assessment by FE model updating: methodology and case studies", *Finite Elements in Analysis and Design*, Vol. 37, No. 10, pp. 761–775.

Cai, C.S. and Shahawy, M. (2003). "Understanding capacity rating of bridges from load tests", *Practice Periodical on Structural Design and Construction*, Vol. 8, No. 4, pp. 209–216.

Chajes, M.J., Mertz, D.R. and Commander, B. (1997). "Experimental load rating of a posted bridge", *Journal of Bridge Engineering*, ASCE, Vol. 2, No. 1, pp. 1–10.

Chowdhury, M.R. and Ray, J.C. (2003). "Accelerometers for bridge load testing", *NDT&E International*, Vol. 36, No. 4, pp. 237–244.

Crisfield, M.A. (1981). "A fast incremental/iteration solution procedure that handles snap-through", *Computers and Structures*, Vol. 13, No. 1–3, pp. 55–62.

Ghosn, M., Moses, F. and Gobieski, J. (1986). "Evaluation of steel bridge using in-service testing", *Transportation Research Record*, No. 1072, pp. 71–78.

Hao, H. and Xia, Y. (2002). "Vibration-based damage detection of structures by genetic algorithm", *Journal of Computing in Civil Engineering*, ASCE, Vol. 16, No. 3, pp. 222–229.

Jauregui, D.U. and Barr, P.J. (2004). "Nondestructive evaluation of the I-40 bridge over the Rio Grande River", *Journal of Performance of Constructed Facilities*, Vol. 18, No. 4, pp. 195–204.

Krauthammar, T. and Hall, W.J. (1982). "Modified analysis of reinforced concrete girders", *Journal of the Structural Division*, ASCE, Vol. 108, No. 2, pp. 457–475.

Kwak, H.G. and Kim, D.Y. (2001). "Nonlinear analysis of RC shear walls considering tension-stiffening effect", *Computer and Structures*, Vol. 79, No. 5, pp. 499–517.

Law, S.S., Ward, H.S., Shi, G.B., Chen, R.Z., Waldron, P. and Taylor, C. (1995). "Dynamic assessment of bridge load-carrying capacity. I", *Journal of Structural Engineering*, ASCE, Vol. 121, No. 3, pp. 478–487.

Lee, J. and Fenves, G.L. (1998). "Plastic-damage model for cyclic loading of concrete structures", *Journal of Engineering Mechanics*, ASCE, Vol. 124, No. 8, pp. 892–900.

MATLAB (2005). *Optimization Toolbox User's Guide*, Version 3, The Mathworks, Inc., Natick, USA.

Nowak, A.A. and Tharmabala, T. (1988). "Bridge reliability evaluation using load tests", *Journal of Structural Engineering*, ASCE, Vol. 114, No. 10, pp. 2268–2279.

Rabczuk, T. and Eibl, J. (2004). "Numerical analysis of prestressed concrete girders using a coupled element free Galerkin/finite element approach", *International Journal of Solids and Structures*, Vol. 41, No. 3, pp. 1061–1080.

Rens, K.L., Nogueira, C.L. and Transue, D.J. (2005). "Bridge management and nondestructive evaluation", *Journal of Performance of Constructed Facilities*, ASCE, Vol. 19, No. 1, pp. 3–16.

Scott, M., Rezaizadeh, A., Delahaza, A., Santos, C.G., Moore, M., Graybeal, B. and Washer, G. (2003). "A comparison of nondestructive evaluation methods for bridge deck assessment", *NDT and E International*, Vol. 36, No. 4, pp. 245–255.

Stallings, J.M. and Yoo, C.H. (1993). "Tests and ratings of short-span steel bridges", *Journal of Structural Engineering*, ASCE, Vol. 119, No. 7, pp. 2150–2167.

Tamai, S., Shima, H., Izumo, J. and Okamura, H. (1988). "Average stress-strain relationship in post yield range of steel bar in concrete", *Concrete Library International*, No. 11, pp. 117–129.

Wang, T. and Hsu, T.T.C. (2001). "Nonlinear finite element analysis of concrete structures using new constitutive models", *Computers and Structures*, Vol. 79, No. 32, pp. 2781–2791.

Warner, R.F., Rangan, B.V., Hall, A.S. and Faulkes, K.A. (1998). *Concrete Structures*, Sydney, Australia.

Xia, Y., Hao, H. and Deeks, A.J. (2007). "Dynamics assessment of shear connectors in slab-girder bridges", *Engineering Structures*, Vol. 29, No. 7, pp. 1475–1486.

Xia, Y., Hao, H., Deeks, A.J. and Zhu, X. (2008). "Condition assessment of shear connectors in slab-girder bridges via vibration measurements", *Journal of Bridge Engineering*, ASCE, Vol. 13, No. 1, pp. 43–54.